RAS 8315

LOCA RESULTS FOR ADVANCED-ALLOY AND HIGH-BURNUP ZIRCALOY CLADDING

Y. Yan, T. Burtseva, and M. C. Billone

Argonne National Laboratory (ANL)
Argonne, Illinois, USA

Abstract

LOCA integral test results are reported for high-burnup BWR cladding ramped in steam from 300°C through ballooning-and-burst to 1204°C, oxidized at 1204°C for 5 minutes (≈20% maximum ECR), and slow cooled. The 300-mm fueled LOCA sample was sectioned for fuel and cladding metallographic imaging, as well as hydrogen and oxygen determination. The measured cladding oxide layer thicknesses in the ballooned region were comparable to the ones measured for a nonirradiated Zry-2 sample tested under the same conditions. Thus, the 10-μm corrosion layer, the fuel-cladding bond and the presence of fuel do not protect the cladding from steam oxidation in the ballooned region. However, the hydrogen pickup in the balloon neck region was low (≈200 wppm), as compared to measured peak values (≈4000 wppm) for the nonirradiated Zry-2 sample. Results are also presented for the oxidation kinetics and post-quench ductility of nonirradiated ZIRLO and M5, as compared to the performance of Zry-4.

Introduction

The LOCA licensing criteria (10 CFR 50.46) limit peak cladding temperature to 2200°F (1204°C) and maximum oxidation (expressed as equivalent cladding reacted, ECR) to 17% to ensure cladding ductility during the emergency-core-cooling-system quench and during possible post-LOCA events (e.g., seismic). In formulating these criteria, it was assumed that the detailed loading modes and magnitudes experienced by the cladding, beyond the thermal stresses induced by rapid cooling, are not well defined. Cladding that retains some plastic ductility has more margin than brittle cladding for surviving quench and post-quench loads without fragmenting Based on Appendix K of this regulation, the Baker-Just (BJ) correlation is to be used to calculate the metal-water (i.e., steam) reaction. Regulatory Guide 1.157 (1989) allows the use of best-estimate correlations, such as Cathcart-Pawel (CP), to calculate the oxidation rate in steam for T > 1900°F (1038°C). At 1204°C, the ratio of the BJ-to-CP prediction is ≈1.3. To compensate for the possible effects of high burnup operation (e.g., hydrogen pickup), NRC Information Notice 98-29 (1998) defines total oxidation to include in-reactor corrosion (ECR_{ss}), as well as transient steam oxidation (ECR_t).

The LOCA integral tests at ANL, using high burnup BWR and PWR fuel-rod segments, are designed to address the adequacy of the embrittlement criteria, of the correlations (CP vs. BJ) used to calculate oxidation, and of the decrease in allowable transient oxidation ($ECR_t \leq 17\% - ECR_{ss}$) to compensate for the embrittling effects of hydrogen. In addition to this confirmatory aspect of the research, the fundamental behavior of high-burnup fuel and cladding, exposed to a LOCA transient, is investigated and characterized. For advanced cladding alloys, the post-quench ductility of nonirradiated

Template = SECY-028

SECY-02

samples is characterized vs. ECR and oxidation temperature (1000-1260°C) and compared to the behavior of Zry-4 and Zry-2, for which an extensive database exists in the open literature.

LOCA-relevant research at ANL includes cladding high-temperature steam oxidation studies [1], LOCA integral testing of fueled segments [2], post-quench ductility testing of LOCA integral specimens, and post-quench ductility testing of nonirradiated zirconium-based cladding alloys (Zircaloy-2, Zircaloy-4, ZIRLO, M5, and E110). Two LOCA integral tests with high-burnup BWR samples (from a Limerick fuel rod at 56 GWd/MTU) were completed in 2002: ramp-to-burst in Ar (ICL#1); and ramp through burst in steam to 1204°C followed by 5 minutes of oxidation and slow cooling (ICL#2). Limerick cladding is Zr-lined Zry-2 (GE-11 9×9 assembly design) with ≈10 μm of in-reactor corrosion, ≈0.7 wt.% oxygen and ≈70 wppm hydrogen. Burst temperatures and pressures, fuel permeability results, profilometry, and burst-opening characteristics were presented at NSRC-2002 [2]. The full LOCA integral test (ICL#3), including quench from 800°C, is scheduled for early 2004. This sequence is indicated schematically in Fig. 1. After completion of the high-burnup BWR test matrix, high-burnup PWR rods (from the H. B. Robinson reactor) will be subjected to the LOCA test sequence indicated in Fig. 1. In this paper, the results of the destructive examinations of the ICL#2 sample are presented: fuel morphology, cladding inner- and outer-surface oxidation within the ballooned region, and hydrogen pickup near the neck region. Advanced-alloy weight gain data and post-quench ductility data are also presented and compared to the performance of Zry-4 for samples oxidized at 1000°C and 1100°C to CP-calculated ECR values ≤20%.

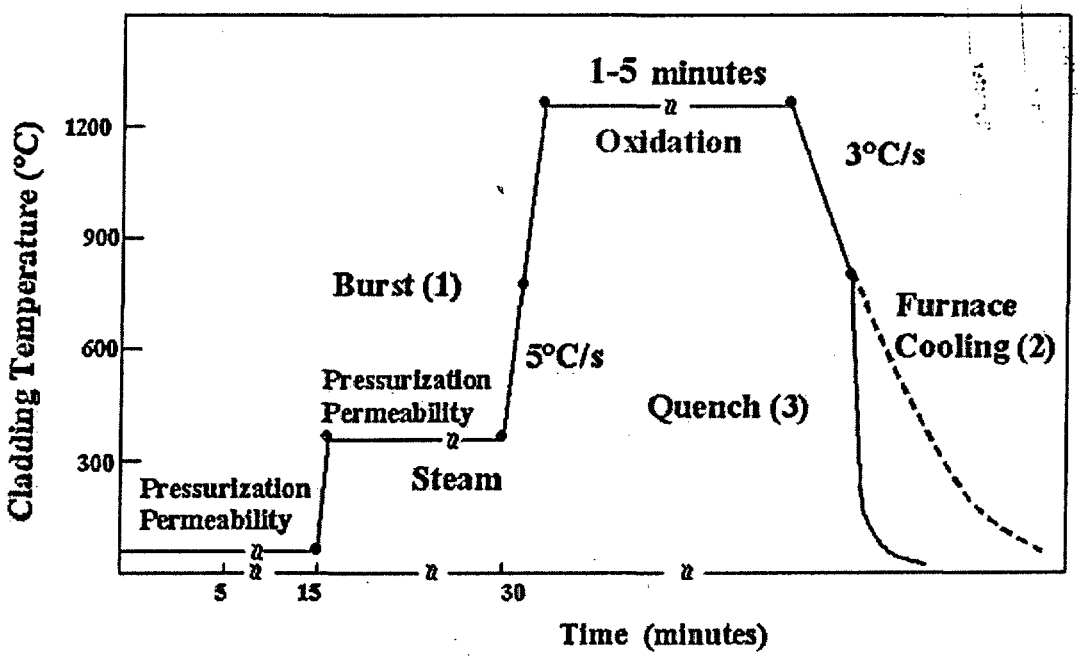

Fig. 1. Temperature histories for the LOCA integral tests: (1) ramp-to-burst test conducted in August 2002; (2) full LOCA sequence up through slow-cooling to 800°C followed by furnace cooling (September 2002); and (3) full LOCA sequence including quench from 800°C to 100°C (2004).

LOCA Out-of-Cell Integral Tests Results: OCL#11 Sample

The out-of-cell LOCA integral apparatus contains the same features as the in-cell apparatus: radiant furnace, argon purge system, high-pressure system to internally pressurize the 300-mm-long test sample, steam supply system, and quench system. Both share the same control and data acquisition systems. The out-of-cell apparatus has been used to generate baseline data for nonirradiated Limerick archival cladding: 9×9 Zry-2, 11.18-mm outer diameter (OD), and 0.71-mm wall thickness. Results for the OCL#11 companion test to ICL#2 are discussed here. Figure 1 shows a schematic of the temperature history for this test (5 minutes at 1204°C), with the dashed line indicating furnace cooling at the end of the test from 800°C to room temperature. Nondestructive results and some destructive results for the ICL#11 sample are reported in Ref. 2.

Additional characterization of the axial distribution of oxygen and hydrogen was performed. Figure 2a shows the concentrations of oxygen (L_O) and hydrogen (L_H), measured by the LECO method after the OCL#11 LOCA test. These concentrations are referenced to the weight of the oxidized samples. The data need to be converted to concentrations referenced to the pre-oxidized sample weight in order to determine pickup values during the transient. Following the weight-gain correction, the as-fabricated oxygen (C_{Oi} = 0.11 wt.%) and hydrogen (C_{Hi} = 5 wppm) contents are subtracted to give oxygen (ΔC_O) and hydrogen (ΔC_H) pickup, referenced to the cladding prior to oxidation. The algorithms for calculating ΔC_O (in wt.%) and ΔC_H (in wppm) from the LECO data (L_O and L_H) are:

$$\Delta C_O = (L_O - C_{Oi})/(1 - L_O/100\%) \quad (1)$$

$$\Delta C_H = (1 + \Delta C_O/100\%)\, L_H - C_{Hi} \quad (2)$$

The ECR (in %) is determined from the oxygen pickup: ECR = 2.85 ΔC_O. However, based on benchmarking tests, it has been shown that ≈10% of the oxygen is lost during LECO sample preparation. Thus, for the ECR calculation "L_O" is replaced by "1.1 L_O" in Eq. 1. In addition, quantitative metallography, along with the CP models for interface oxygen concentrations and diffusion within the oxide, alpha and beta layers, was used to determine oxygen concentration, weight gain, and the corresponding ECR. The axial distributions of ECR and hydrogen pickup are shown in Fig. 2b. As expected, the oxygen pickup and ECR peak at the center of the burst region where the cladding is thinnest and the oxidation is fully two-sided. The ECR decreases away from the burst center as the cladding wall thickness increases and the degree of inner-surface oxidation decreases. Also, as expected, the hydrogen pickup, due to secondary hydriding, peaks near the balloon neck regions. The magnitude of these hydrogen peaks, however, is larger than previously reported [3] and may depend on the details of ballooning strain profile, burst opening, diameter of pellets (zirconia) inside the cladding, heating method (internal vs. external vs. direct-electrical) and cladding type (lined Zry-2 vs. Zry-4). As these hydrogen peaks, as well as the hydrogen within the balloon region, are potentially embrittling, it is important to determine the magnitude of such effects for high-burnup cladding.

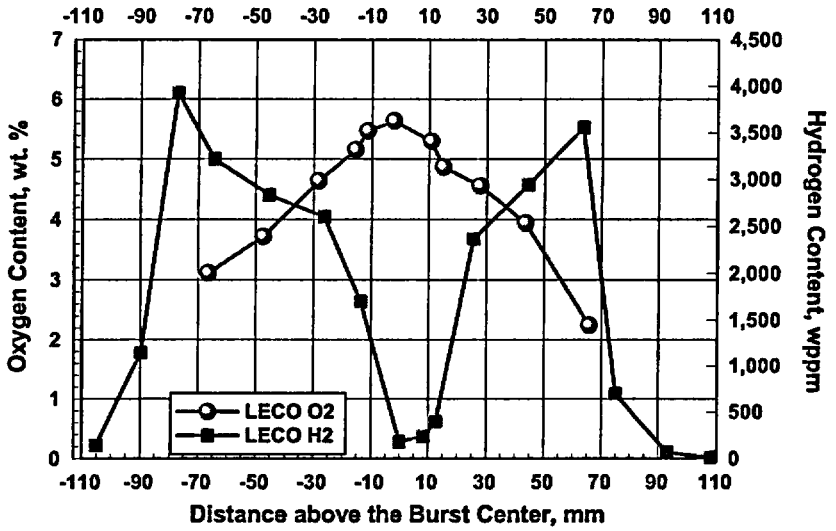

(a)

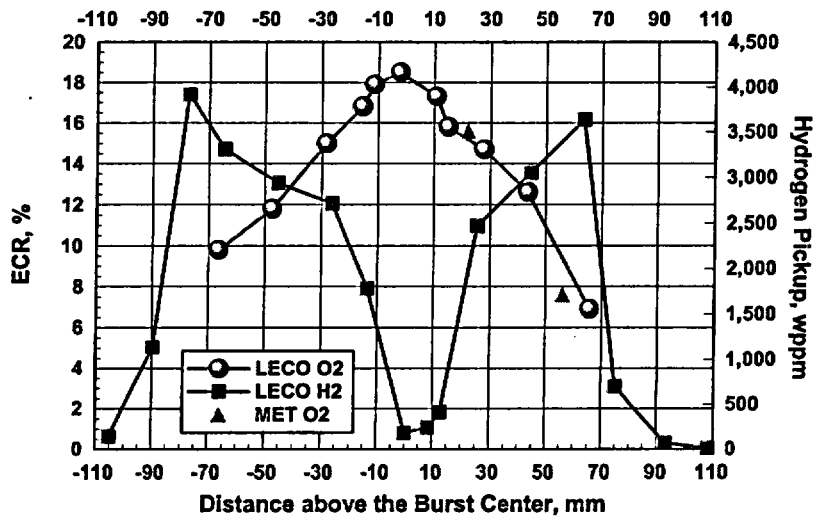

(b)

Fig. 2. Axial distributions of oxygen, hydrogen and ECR for out-of-cell test OCL#11 sample with nonirradiated Zry-2 cladding: (a) LECO data for concentrations referenced to the weight of the oxidized samples; and (b) data corrected for weight gain and pre-transient concentrations of oxygen and hydrogen. Oxygen concentrations in the oxide and alpha layers are much higher than the measured average value, while hydrogen concentration in the prior-beta layer is much higher than the measured average value.

LOCA In-Cell Integral Test Results: ICL#2 Test Sample

Background

The ICL#2 test was conducted in September 2002. Nondestructive characterization (photography, profilometry, etc.) was completed shortly after the test. The results were reported at NSRC-2002 [2] and are summarized in Table 1. During the post-test handling, some fuel particles (<0.3 mm in size) fell out through the burst opening. The mass of particles collected represents <25% of one fuel pellet. In October 2002, the hot cells were closed for significant maintenance and repair. Movement of radioactive material was required to do the repairs. In preparation for the movement of the ICL#2 sample, the burst area was epoxied. As the epoxy was applied very quickly, some of it spread through much of the balloon region. The consequences of the epoxy are twofold: fuel particles present about a month after post-test sample handling were "frozen" in position; and no hydrogen analyses of the cladding could be performed within the ballooned region because of the high hydrogen content of the epoxy and the difficulty of removing the fuel-embedded epoxy.

Axial Locations of Samples Sectioned for Destructive Evaluation

Figure 3 shows the axial locations from which the fuel and cladding metallography samples and the hydrogen-analysis samples were sectioned relative to the burst opening location and the ballooning strain. Oxygen-analysis samples were also prepared next to the H_1 and H_2 locations.

Fuel Morphology

There is considerable interest in the behavior of high-burnup fuel during a LOCA transient. Prior to the transient, the fuel is tightly bonded to the cladding. During ballooning, the cladding pulls away from the fuel. This allows space for fuel particles (macro-cracked, micro-cracked, and very small particles from the rim layer) to fall into the balloon region. If such movement were to result in a local increase in fuel per unit length, then the higher decay heat per unit length would cause an increase in cladding oxidation temperature and maximum ECR in the burst region. Also, if the fuel-cladding bond material moves with the cladding, such a layer could slow down the initial steam oxidation rate and could protect the cladding from the large hydrogen absorption observed in tests with bare-wall, nonirradiated cladding (see Fig. 2). As methods that could be used to freeze the fuel particles in place (e.g., epoxy) conflict with cladding characterization, the ANL program is more focused on the details of cladding oxidation, hydriding, and ductility than on fuel behavior. This was certainly the case for the ICL#2 sample, as no attempt was made to prevent fuel fallout during handling. In future tests, the burst area will be taped following the test to minimize fuel fallout and the samples will be gamma-scanned – prior to other nondestructive characterization – to determine the axial distribution of fuel in and beyond the balloon region. For ICL#2 axial locations with little-to-no permanent strain, metallographic images of the fuel most likely represent the condition of the fuel at the end of the LOCA test. For the ICL#2 balloon region, it is likely that significant redistribution of fuel particles took place between the end of the LOCA test and the filling of this region with epoxy.

Table 1 Comparison of Results from In-Cell Test ICL#2 and Out-of-Cell Test OCL#11. Samples were ramped from 300°C to 1204°C in steam, held for 5 minutes at 1204°C, cooled at 3°C/s to 800°C and furnace-cooled to room temperature.

Parameter	ICL#2	OCL#11
Environment	Steam	Steam
Hold Temperature, °C	1204	1204
Hold Time, minutes	5	5
$(P_g)_{max}$, MPa	8.87	8.61
T at $(P_g)_{max}$, °C	728	680
Burst Pressure (P_B), MPa	≤8.01	≤7.93
Burst Temperature (T_B), °C	≥750	753±22
Burst Center Relative to Specimen Midplane, mm	+25	+35
Burst Shape	Oval	Dog Bone
Burst Length, mm	14	11
Max. Burst Width, mm	3.5	1
Length of Balloon, mm	90	140
$(\Delta D/D_o)_{max}$[a], %	39±10	43±10
Reference Minimum Wall Thickness for ECR, mm	≈0.514	≈0.500
Maximum ECR, %		
Calculated	≈20	≈20
Measured	---	19

[a]From profilometry at 0° and 90° relative to burst opening

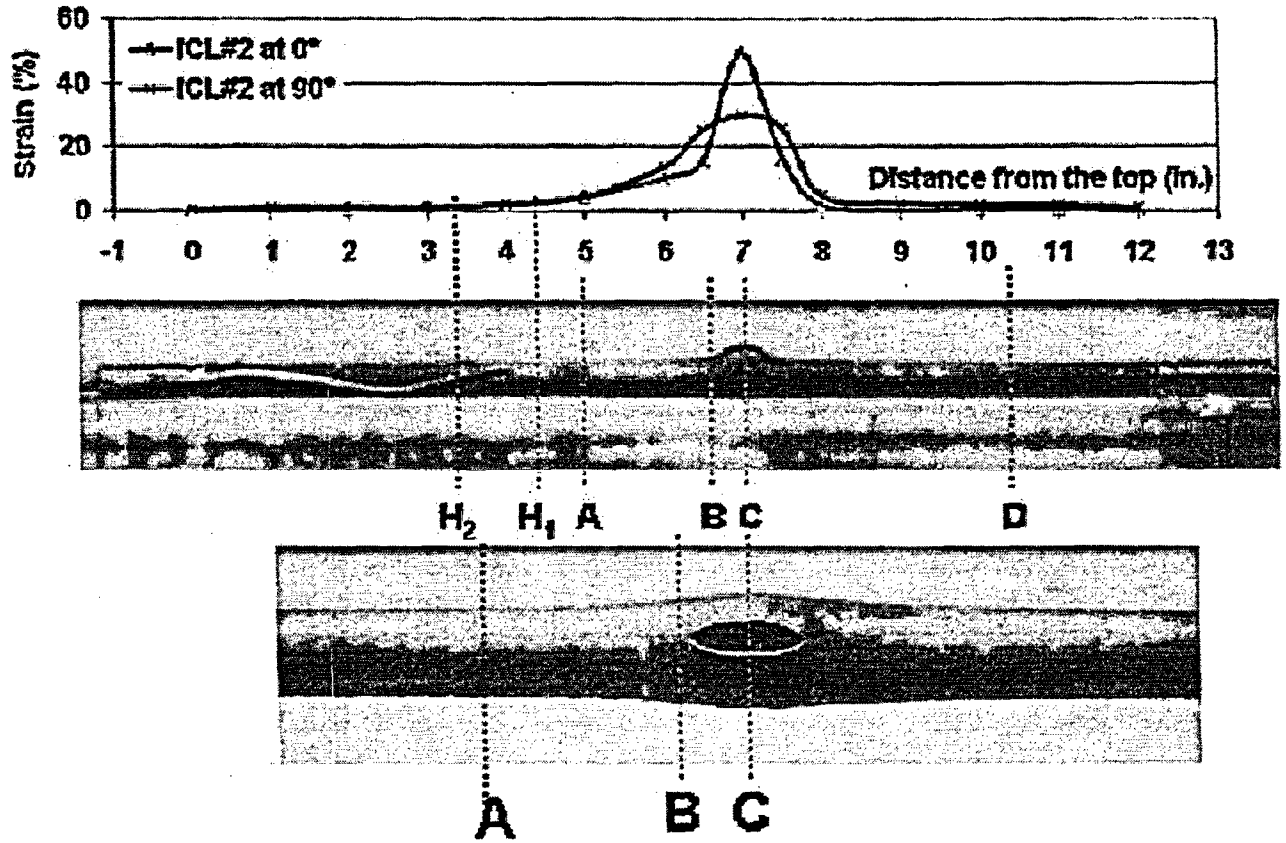

Fig. 3. Sectioning diagram for high-burnup-BWR LOCA sample ICL#2. Hydrogen, as well as oxygen, measurements were taken at locations H_1 and H_2.

Figure 4 shows the fuel structure ≈130 mm below the burst center (45 mm above the bottom endcap), as compared to the fuel structure of the as-received Limerick fuel. The structures are similar, except that the post-LOCA fuel shows a ring of circumferential tearing about mid-radius. This tearing may have occurred as the cladding tried to move a small distance (0-0.1 mm) away from the fuel and/or because of the effects of fission-product gases on the fuel (see dark ring near mid-radius for the pre-LOCA fuel in Fig. 4a). Figure 5a shows a high-magnification of a small area of the mid-radius of the Limerick pre-LOCA fuel with the high concentration of fission gas within the grains, as well as some fission gas bubbles on grain boundaries. Figure 5b shows an enlargement of the region of post-LOCA fuel with the circumferential tearing.

Figure 6 shows low-magnification images of the fuel structure at: (a) ≈50 mm above the burst (axial position A in Fig. 3) and (b) ≈12 mm above the burst center (axial position B in Fig. 3). At ≈50 mm above the burst, the circumferential tearing is enhanced as compared to the ≈130-mm location, most likely due to the larger cladding strain. Some fuel fallout, which may have occurred during cutting is observed, although this region of the fuel column was embedded in a soft epoxy prior to cutting. Smaller fuel particles are also observed. In Fig. 6b, a wide range of fuel-particle sizes is observed, although these particles and fuel chunks are not co-planar. The particles and chunks are held in place by soft epoxy. Because this photograph was taken after extensive handling of the sample, resulting in axial redistribution of particles and fuel fallout through the burst opening, it does not represent the fuel condition near the burst center during the LOCA test or after cooldown. The most that one can glean from such a picture is that the wide range of fuel-particle sizes would allow some fuel to fall from <50 mm above the burst center to the burst region.

Cladding Metallography

Low-magnification photographs were taken at 10 circumferential locations of the burst midplane and pieced together (see Fig. 7) to obtain an image of the metal (oxygen-stabilized alpha and prior-beta) thickness vs. circumferential location. The inner and outer oxide layers are not visible in Fig. 7. Also, the burst tips, which are very thin and heavily oxidized are likely lost in the cutting process. However, the low-magnification image is consistent with the higher-quality images taken of the companion out-of-cell sample (OCL#11): thin metal wall near the burst opening, which increases in thickness as the circumferential position increases to 180° from the burst opening. High-magnification micrographs were obtained of the inner and outer cladding regions away from the burst tips. These are shown in Figs. 8a (outer surface) and 8b (inner surface). The thickness of the outer-surface oxide layer is consistent with CP-calculated oxide thickness and consistent with the results of oxidation tests conducted on undeformed cladding samples [2]. The results demonstrate that the ≈10-μm-thick corrosion layer is not protective with regard to steam oxidation. The inner-surface oxide layer is wavy in appearance, which may be due to the high hydrogen-to-steam ratio within the burst region. It is comparable in thickness to the outer-surface layer, which suggests that the fuel-cladding bond layer is also non-protective with regard to steam oxidation. Alpha incursions into the prior-beta layer are observed at this location, just as they were observed in the oxidation tests [1,2]. These most likely formed during the 3°C/s cooling from 1200°C to 800°C. They represent regions with higher oxygen content than the remaining prior-beta material and lower oxygen content than the alpha layer formed at 1200°C.

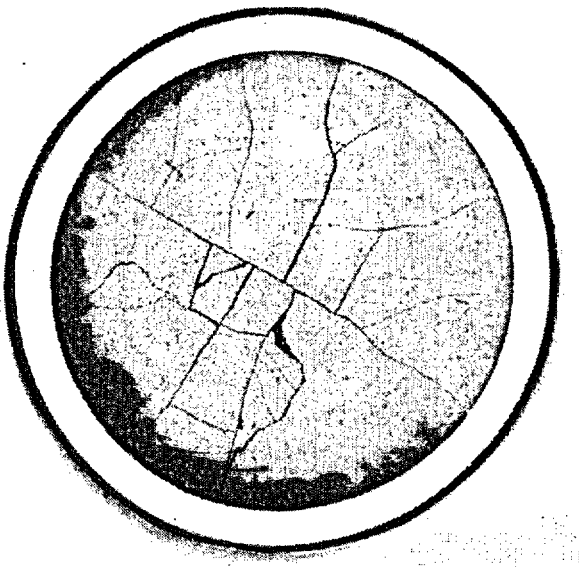

(a)

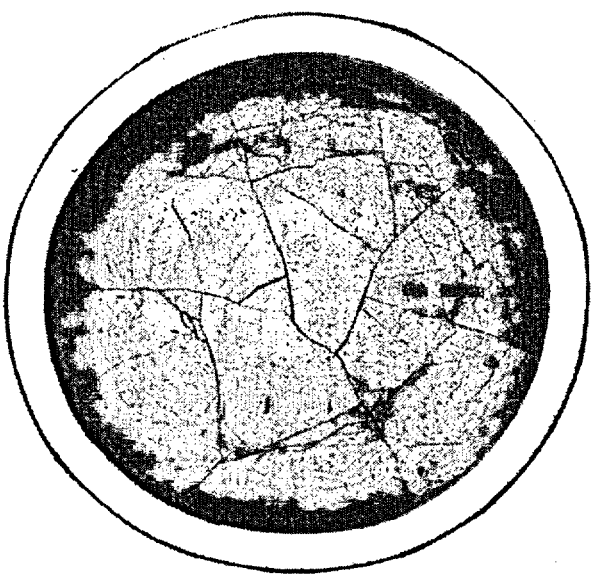

(b)

Fig. 4. Low-magnification images of the Limerick fuel prior to LOCA testing (a) and after LOCA test ICL#2 (b). The location of the pre-LOCA fuel is 180 mm from the LOCA sample. The post-LOCA fuel is ≈130 mm below the ICL#2 burst center and ≈45 mm from the lower endcap – axial location D in Fig. 3.

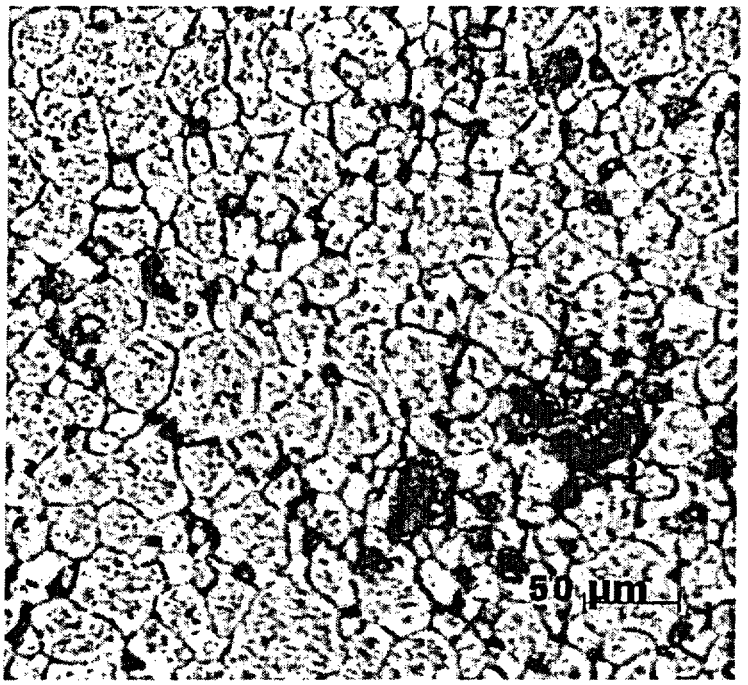

(a)

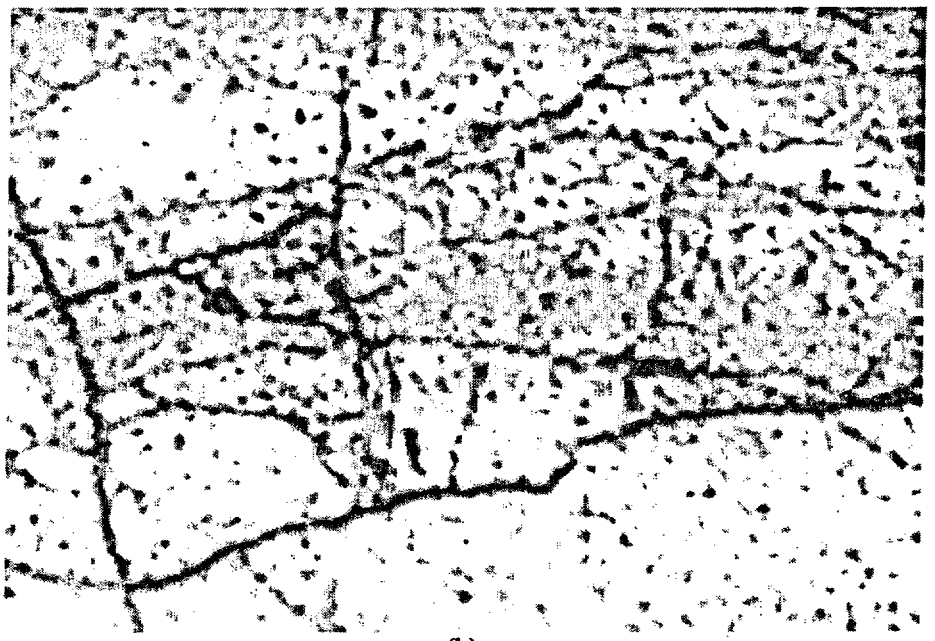

(b)

Fig. 5. High-magnification of pre-LOCA-fuel mid-radius showing high concentration of fission gas within the grains (a) and enlargement of the post-LOCA fuel mid-radius region showing circumferential tearing (b) – axial location D in Fig. 3.

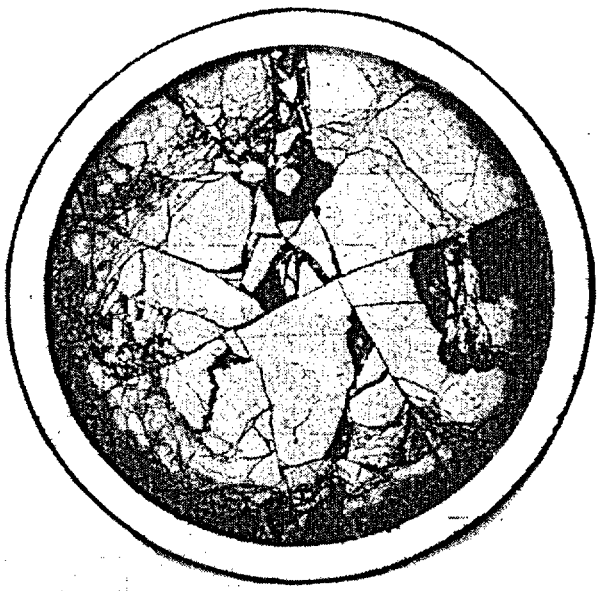

(a)

(b)

Fig. 6. Fuel morphology of ICL#2 sample at ≈50 mm above burst center (a) – axial location A in Fig. 3 – and ≈12 mm above burst center (b) – axial location B in Fig. 3. Cladding diametral strains are 2-4% for the Fig. 6a cross-section and 15-25% for the Fig. 6b cross-section.

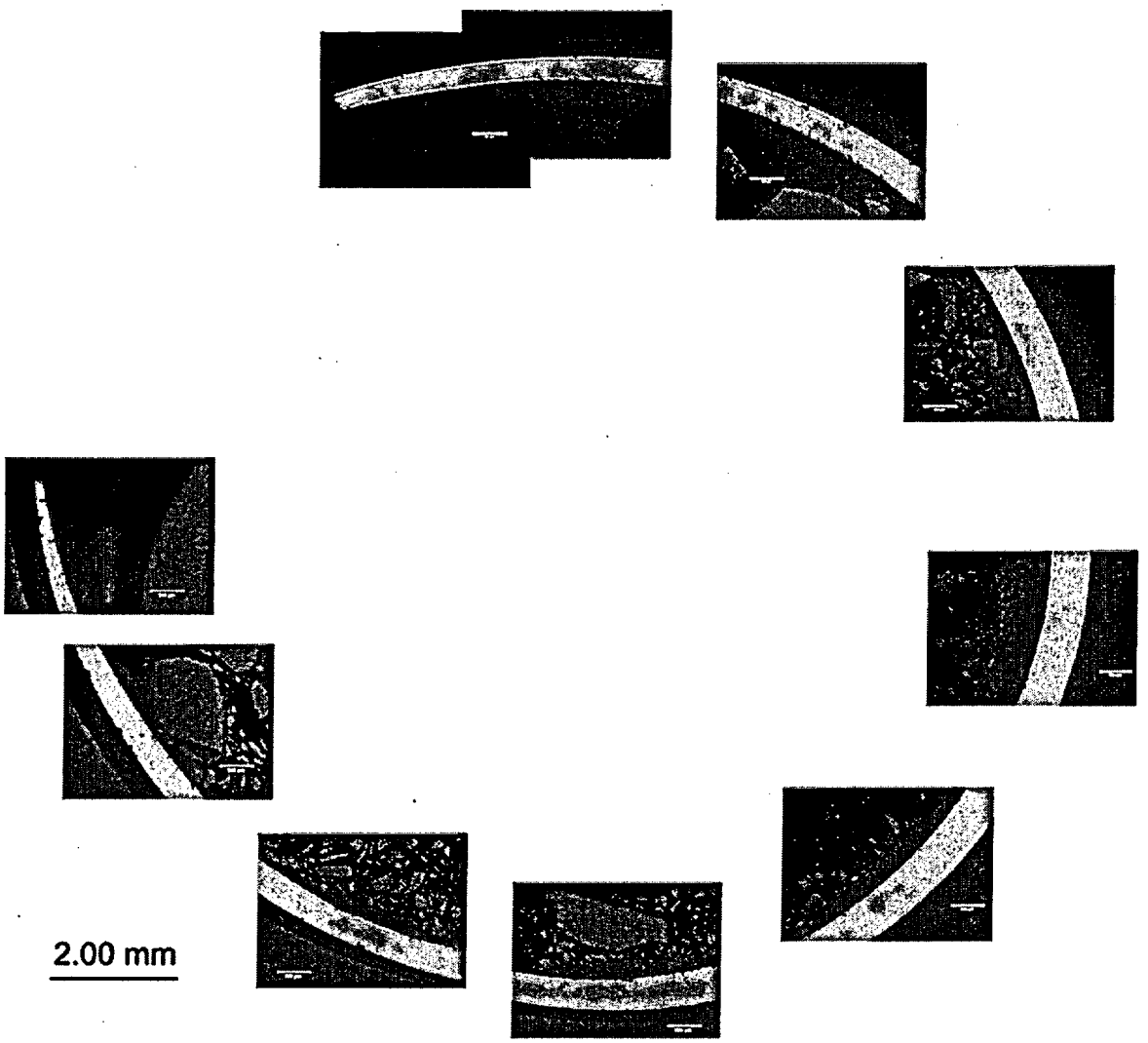

Fig. 7. Low-magnification composite of the cladding metal (alpha and prior-beta) cross-section at the burst midplane of the ICL#2 sample – axial position C in Fig. 3. Cladding diameter increase from burst opening to 180° from burst opening is ≈50%. Diameter increase ±90° from burst opening is ≈30%. Fuel particles embedded in epoxy can also be observed.

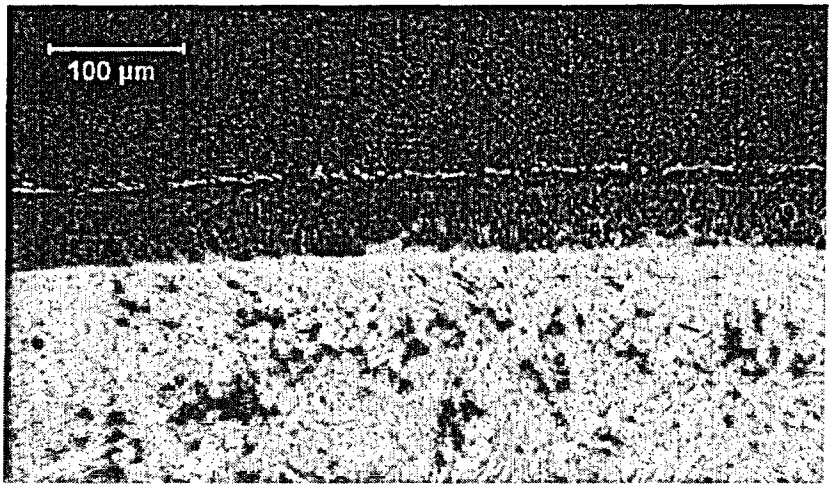

(a)

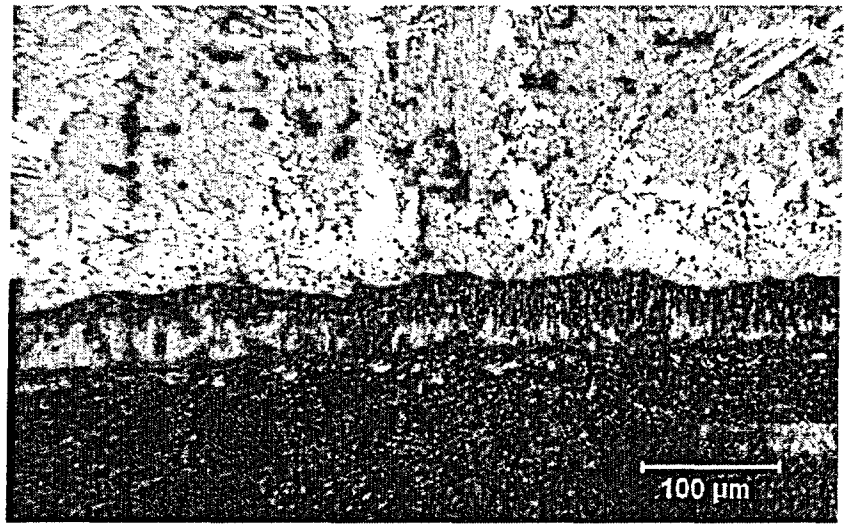

(b)

Fig. 8. Outer (a) and inner (b) cladding oxide layers ≈180° from burst center – axial position C in Fig. 3. These etched samples show oxygen-stabilized alpha incursions into the prior-beta layer.

More detailed metallography was obtained at axial position B (≈12 mm above the burst midplane). Figures 9a-b show the images of the arc segment after etching. Double-sided oxidation is evident at this location, with the inner-surface oxide thickness ≥ the outer-surface oxide thickness. Eight such regions were imaged around the cladding at axial location B, and quantitative metallography was performed to determine the distribution of cladding thickness, outer-surface oxide layer thickness and inner-surface oxide layer thickness with respect to circumferential orientation. These results (b) are compared in Fig. 10 to the baseline results obtained for the nonirradiated Zry-2 sample used in the OCL#11 test (a). In order to focus on the transient oxidation of the high-burnup LOCA sample (ICL#2), 10 μm was subtracted from the total outer-surface oxide-layer thickness to generate the transient oxidation data. Notice that the oxide layer thicknesses shown in Fig. 10 were multiplied by 7 to allow them to be plotted on the same scale as the wall thickness. For the OCL#11 sample, the oxide layers formed on the inner- and outer-cladding surfaces are consistent with respect to circumferential orientation. Average values for outer- and inner-surface oxide layer thicknesses for OCL#11 are 59 μm and 56 μm, respectively. The weight gain and ECR were determined to be 11.4 mg/cm^2 and 15.7%, respectively, while the prior-beta layer thickness was measured to be 398 μm. The high-burnup sample differs somewhat in that there is more circumferential variation in the inner-surface oxide-layer thickness. The average outer- and inner-surface oxide layers are 55 μm and 57 μm, respectively. The weight gain and ECR were determined to be 10.5 mg/cm^2 and 14.9%, respectively, while the prior-beta layer thickness was measured to be 435 μm for the ICL#2 sample at this location. Although the axial locations with respect to the burst center are slightly different (18 mm above for OCL#11 and 12 mm above for ICL#2), the values for oxide layer thickness, weight gain, ECR, and prior-beta layer thickness are remarkably close. These results indicate that close to the burst region the steam oxidation of nonirradiated and high-burnup Zry-2 samples is essentially the same. No high-burnup effects were observed.

Secondary Hydriding

Hydrogen is released during inner-surface oxidation within the balloon region, particularly near the burst region. Because of the flow resistance of the small burst opening, a relatively high fraction of this hydrogen remains within the sample and migrates up and down the sample towards the balloon neck-and-beyond regions. For the nonirradiated samples, there is little resistance to this migration and the bare cladding inner surface absorbs a large amount of hydrogen (see Fig. 2). Qualitatively, the same behavior would be expected for fresh and low-burnup fuel cladding. For high-burnup fuel, the axial extent of hydrogen that could come in contact with the cladding would be limited by the presence of the fuel, and the local hydrogen absorption would be limited by the fuel-cladding bond layer. Although this layer has been shown to be non-protective with regard to steam oxidation, it is of great interest to determine whether or not it is protective with respect to hydrogen diffusion into the cladding. Hydrogen and oxygen concentrations were measured for ICL#2 samples sectioned from ≈70 mm (axial position H_1 in Fig. 3) and ≈90 mm (axial position H_2 in Fig. 3) above the burst center. The raw data give oxygen and hydrogen concentrations of L_O = 2.92 wt.% and L_H = 230 wppm, respectively, at H_1 and L_O = 2.78 wt.% and L_H = 284 wppm, respectively, at H_2. Using these data, hydrogen pickup and ECR values were determined to be: ΔC_H = 167 wppm and ECR = 7.4% at H_1, and ΔC_H = 220 wppm and ECR = 6.9% at H_2. These results are compared in Fig. 11 to the peak hydrogen-content locations and values for OCL#11, relative to the average diametral strain. It is clear that the high-burnup-cladding values are significantly lower than the nonirradiated-cladding values at comparable cladding strain values. This shows a significant difference in the behavior of high-burnup-fueled vs. nonirradiated cladding More data are needed to map out the axial distribution of hydrogen in post-LOCA high-burnup cladding.

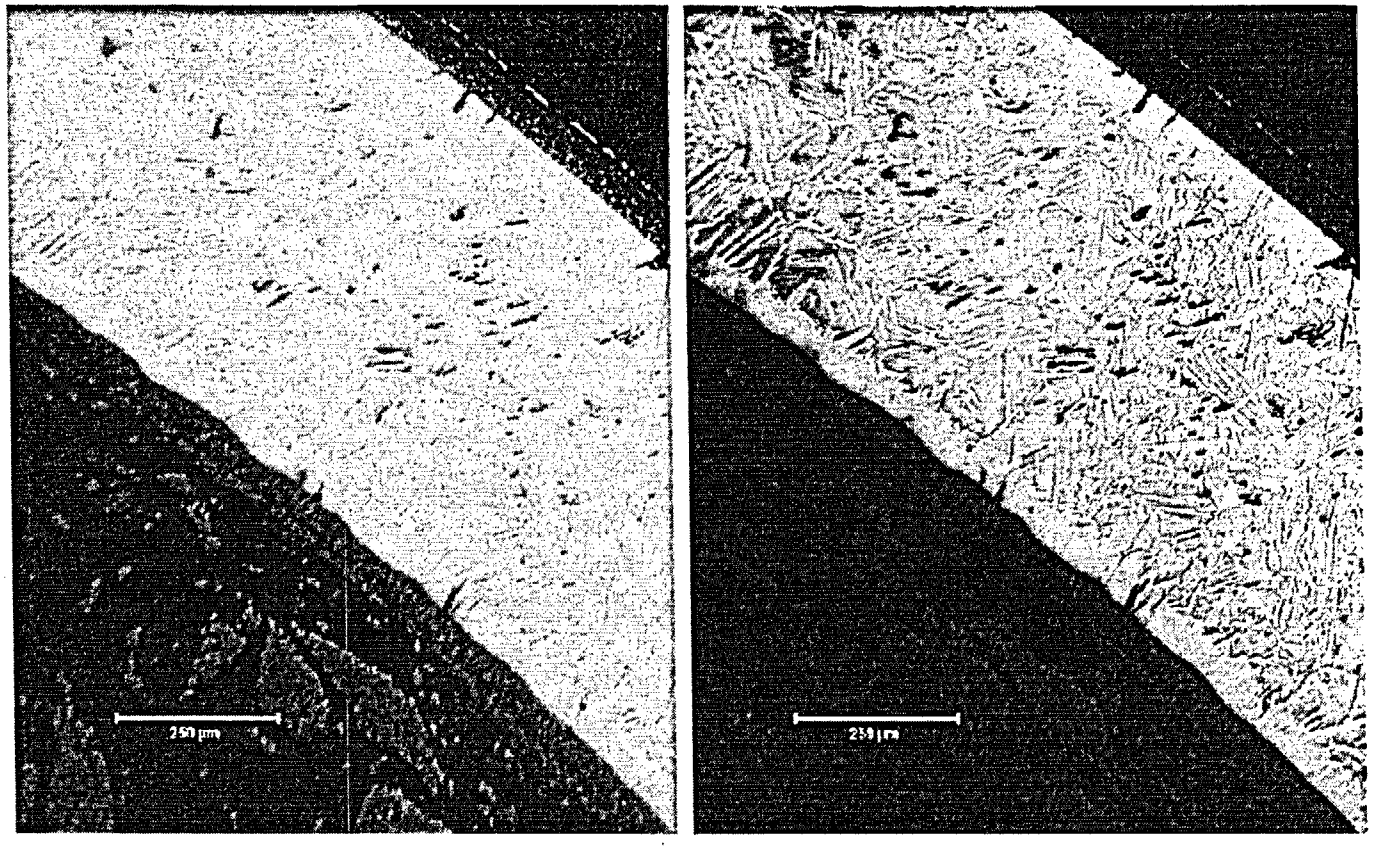

(a) (b)

Fig. 9. Metallographic images of the cladding ≈12 mm above the burst midplane. The micrograph (a) shows good definition of the inner- and outer-surface oxide layers; and the micrograph (b) shows well-defined alpha layers that formed at 1200°C and large prior-beta grains surrounded by oxygen-stabilized alpha layers formed during slow cooling to 800°C.

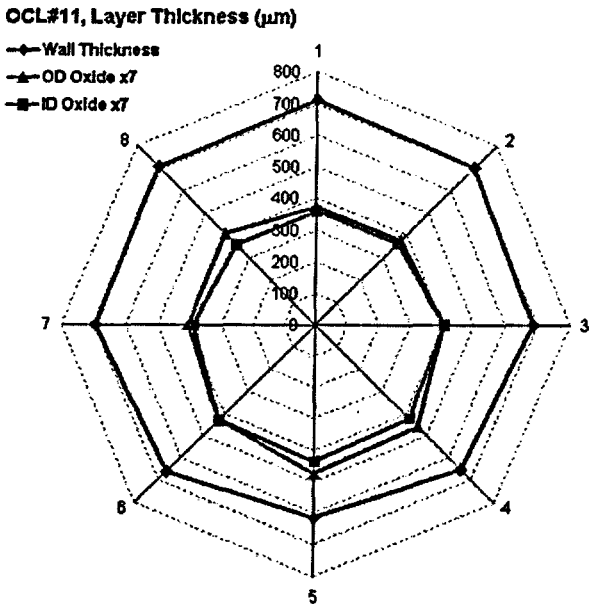

(a)

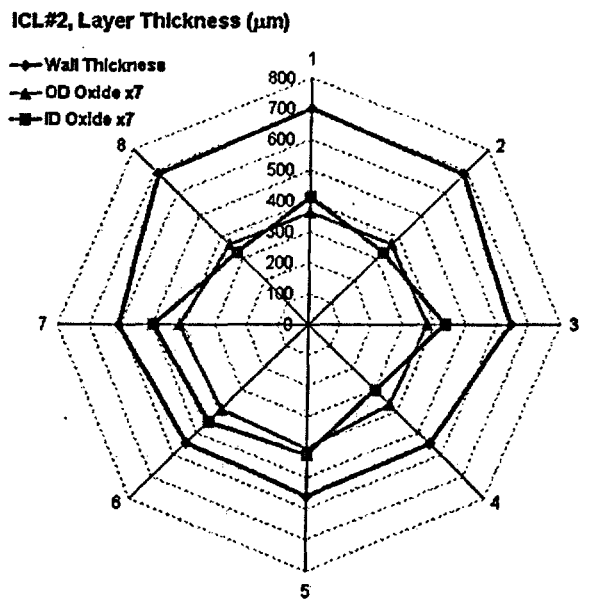

(b)

Fig. 10. Circumferential variation in post-LOCA cladding wall thickness, outer-surface (OD) oxide-layer thickness, and inner-surface (ID) oxide layer thickness for : (a) nonirradiated OCL#11 Zry-2 sample 18 mm above burst center; and (b) high-burnup ICL#2 Zry-2 sample 12 mm above burst center.

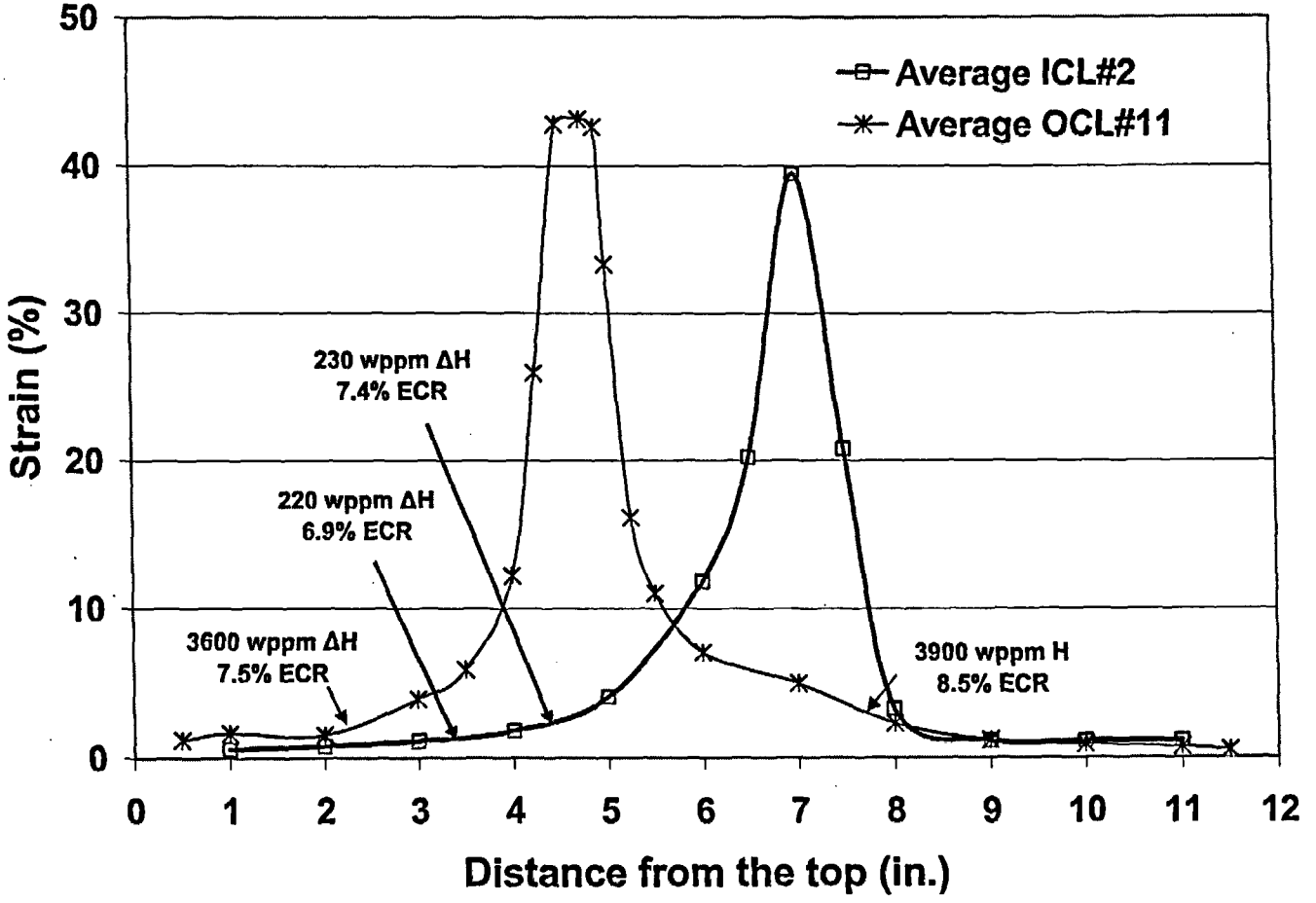

Fig. 11. Hydrogen pickup and ECR distributions for post-LOCA ICL#2 high-burnup-fueled Zry-2 sample as compared to hydrogen peaks in post-LOCA OCL#11 nonirradiated Zry-2 sample (see Fig. 2).

Advanced-Alloy Cladding Post-Quench-Ductility Results

The purpose of this program is to determine the post-quench ductility of advanced cladding alloys ZIRLO and M5, as compared to the post-quench ductility of Zry-4. While extensive literature data are available for traditional Zircaloy claddings (Zry-4 and Zry-2), relatively little data have been published for ZIRLO and M5. Also, the published data [4, 5] for advanced alloys were generated in different laboratories by very different methods. In this program, all samples are oxidized in the same apparatus at the same ramp rates, hold times, and cooling rates (slow-cooled to 800°C and water-quenched). The 25-mm-long samples are exposed to two-sided steam oxidation prior to cooling. Also, the samples are compressed in the same Instron machine, and the load-displacement data are analyzed by a common method to determine ductility.

The Zry-4 and ZIRLO tubing (17×17 PWR) provided by Westinghouse has an outer diameter of 9.50 mm and a wall thickness of 0.57 mm. The M5 tubing (17×17 PWR) provided by Framatome has an outer diameter of 9.50 mm and a wall thickness of 0.61 mm. Table 2 summarizes the test matrix for oxidizing the samples prior to ring-compression, post-quench ductility testing. The times listed are the equivalent isothermal times at the test temperature to give Cathcart-Pawel (CP) calculated ECR values of 5, 10, 15, 17, and 20%, for an assumed wall thickness of 0.57 mm. Actual ECR values vary depending on the measured weight gain and non-oxidized wall thickness for each sample.

Following oxidation and quench, 8-mm rings are cut from near the middle of the 25-mm-long samples. Ring compression tests are performed at room temperature and a cross-head displacement rate of 2 mm/min. The load-displacement curves are analyzed by the traditional offset-displacement method. The offset displacement, which is often used as the measure of permanent displacement, is normalized to the outer diameter (9.50 mm) to give a nominal plastic hoop strain. Samples that exhibit offset strains >2% are considered to be ductile. However, for samples with ≤2% offset strain, another method is used to better determine permanent deformation and ductility. For this second method, the sample is unloaded after the first significant load drop indicating through-wall failure along the length of the sample. The post-test diameters along and normal to the loading direction are measured directly and compared to the pre-test diameter to give a direct measure of permanent strain. For these low-offset-strain samples, the permanent diameter change in the loading direction is used as the direct measure of ductility.

Oxidation and quench have been completed for Zry-4, ZIRLO and M5 samples oxidized at 1000°C and 1100°C. Weight gains were recorded for each sample, normalized to the oxidation surface area, and compared to CP predictions (in mg/cm^2). Ring-compression tests have also been completed on 8-mm-long rings cut from the oxidation samples. Metallography, microhardness, and hydrogen-content analyses are in progress for the highest ECR samples for each alloy. This characterization is performed to allow correlation between the ductility observed in the ring compression test and the material structure (e.g., prior-beta-layer thickness, extent of alpha incursions into this layer, etc.) and the hydrogen content. Results for E110 oxidized at 1000°C are reported in Ref. 6.

Table 2 Test Matrix for Oxidation of Samples for Post-Quench Ductility Tests. The times and ECR values listed correspond to those calculated using the Cathcart-Pawel weight gain correlation, a nominal wall thickness of 0.57 mm, and two-sided isothermal oxidation in steam. The relationship between ECR (%) and normalized weight gain (Δw in mg/cm^2) is ECR = 1.538 Δw for 0.57-mm-thick cladding samples.

Temperature °C	ECR %	Equivalent Oxidation Time s
1000	5	210
	10	841
	15	1892
	17	2430
	20	3364
1100	5	67
	10	266
	15	599
	17	769
	20	1065
1200	5	25
	10	99
	15	222
	17	285
	20	394
1260	5	14
	10	58
	15	130
	17	167
	20	231

Weight Gain Kinetics

The weight gain data for Zry-4, ZIRLO and M5, oxidized at 1100°C, were in excellent agreement with each other and the CP-predicted weight gain values. These results are consistent with published data for ZIRLO vs. Zry-4 [4] and M5 vs. Zry-4 [5]. At the highest test time, measured values were 13.2 mg/cm^2 (Zry-4), 13.7 mg/cm^2 (ZIRLO), and 13.3 mg/cm^2 (M5), as compared to the predicted value of 13.0 mg/cm^2. Using the measured wall thickness for each alloy, these weight-gain values convert to "measured" ECR values of 20.3% (Zry-4), 21.1% (ZIRLO) and 19.1% (M5).

After oxidation at 1000°C, the weight gain of ZIRLO tracks well with the CP-predicted values up through 17% ECR and is low by only 10% at the highest test time (≈3400 s). Beyond ≈10% CP-ECR, the Zry-4 weight-gain values are 9-13% higher than the CP-values. Consistent with previous work [5], the M5 weight gain is ≈30% lower than the CP prediction and ≈36% lower than the Zry-4 data point at the highest test time. The ECR values determined from the weight gains and the as-received cladding wall thicknesses are: 22.4% (Zry-4), 18.0% (ZIRLO) and 13.3% (M5). In order to further explore these differences in weight gain, metallography was performed on as-polished and etched samples oxidized at 1000°C for ≈3400 s. Figure 12 shows a comparison between as-polished samples of Zry-4 and ZIRLO after this long test time. The inner/outer oxide layer thicknesses are 83-μm/82-μm for Zry-4 and 57-μm/66-μm for ZIRLO, based on quantitative analysis of eight arc segments around the circumference of the samples. The ratio of total oxide thickness is ZIRLO/Zry-4 = 0.75, while the ratio of weight gains is 0.80. Thus, the higher weight gain of Zry-4 at 1000°C and ≈3400 s is a direct result of the thicker oxide layers formed on the Zry-4 inner and outer surfaces.

Figure 13 shows a comparison between as-polished Zry-4 and M5 samples oxidized at 1000°C for ≈3400 s. Based on averaging the oxide layer thicknesses for eight circumferential arc segments, the M5 outer/inner oxide layer thicknesses are 36-μm/32-μm. The ratio of total oxide thickness is M5/Zry-4 = 0.41, while the weight gain ratio is 0.64. Thus, the primary reason for the lower weight gain of M5 as compared to Zry-4 is the relatively slow growth of the inner and outer oxide layers. However, these results also suggest that the alpha and prior-beta regions of M5 pick up more oxygen than Zry-4 for long oxidation times at 1000°C. The results are consistent with the observation that thicker oxide layers are more effective diffusion barriers than thin oxide layers.

Post-Quench-Ductility Results

The load-displacement curves from the ring compression tests were analyzed by the offset method. Figure 14 illustrates this method for a Zry-4 ring oxidized at 1100°C to a CP-calculated ECR of 15% and a measured ECR of ≈16%. The sample fractured into four pieces with the first though-wall fracture occurring at the load or support point. The offset displacement (0.516 mm) prior to the first through-wall crack is determined by mathematically by unloading the specimen at the elastic loading-stiffness rate. Normalizing this offset displacement to the as-fabricated outer diameter (9.50 mm) gives an offset strain of 5.4%. For samples oxidized at 1100°C to a CP-calculated ECR value of ≈17% (≈21% BJ-ECR), the ductility determined by offset strain was in the range of 4-5%. For samples oxidized at 1000°C to ≈17% CP-ECR (≈19% BJ-ECR), the offset-strain ductility was 4-5% for Zry-4 and ZIRLO and >5% for M5. It is interesting to note that all three alloys oxidized at 1000°C to ≈20% CP-ECR (≈22% BJ-ECR) had a post-quench ductility of ≈3%, even though their ECR values determined from measured weight gain and sample thickness range from 22.4% for Zry-4 to 18.0% for ZIRLO to 13.3% for M5. Thus, the post-quench ductility of these alloys oxidized at 1000°C correlates better with time-at-temperature or predicted ECR, which varies as the square-root of time, than with measured ECR.

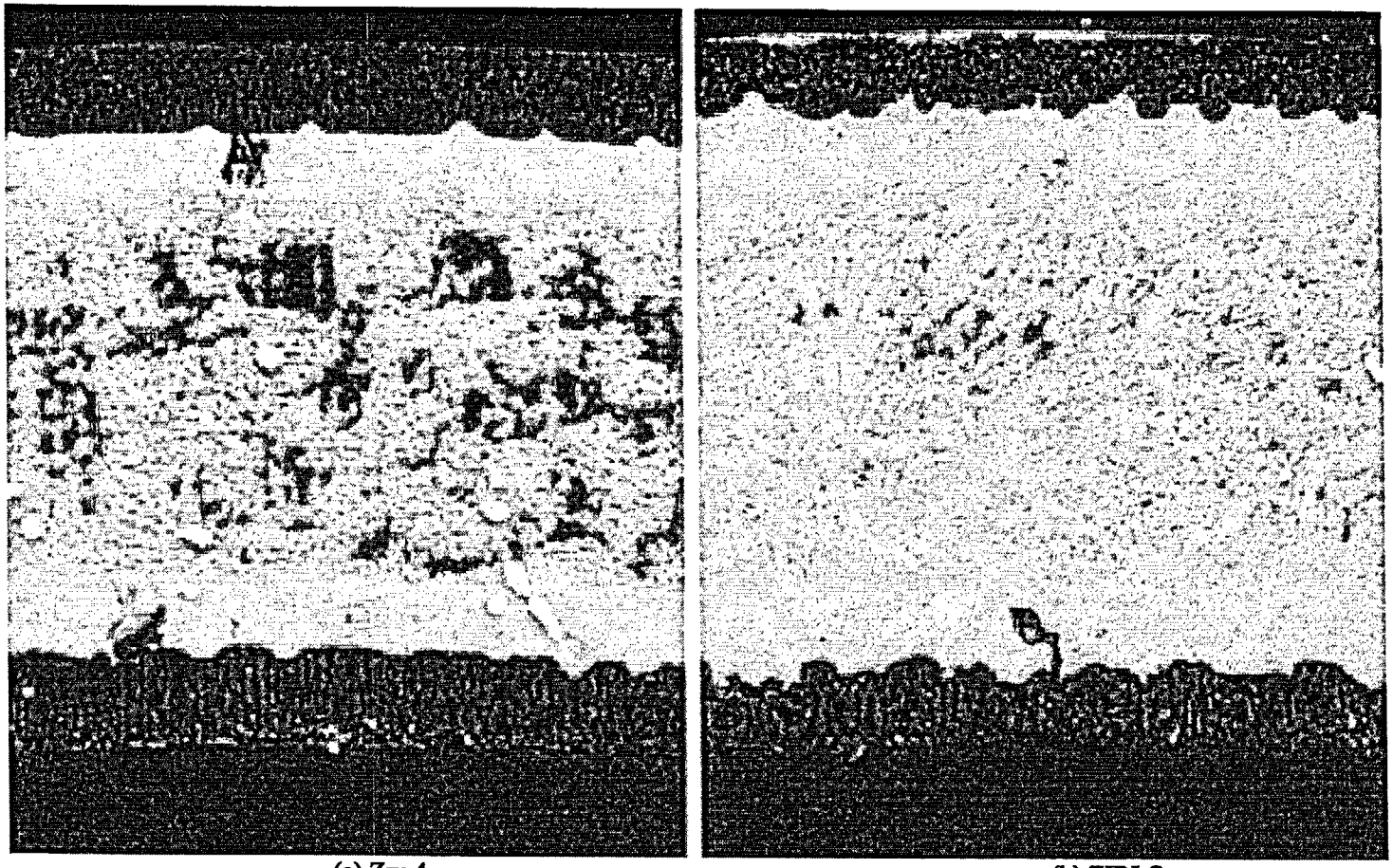

(a) Zry-4 (b) ZIRLO

Fig. 12. Metallography of as-polished Zry-4 (a) and ZIRLO (b) oxidized in steam at 1000°C for ≈3400 s, slow cooled to 800°C and water quenched. Measured ECR values are 22.4% for Zry-4 and 18.0% for ZIRLO.

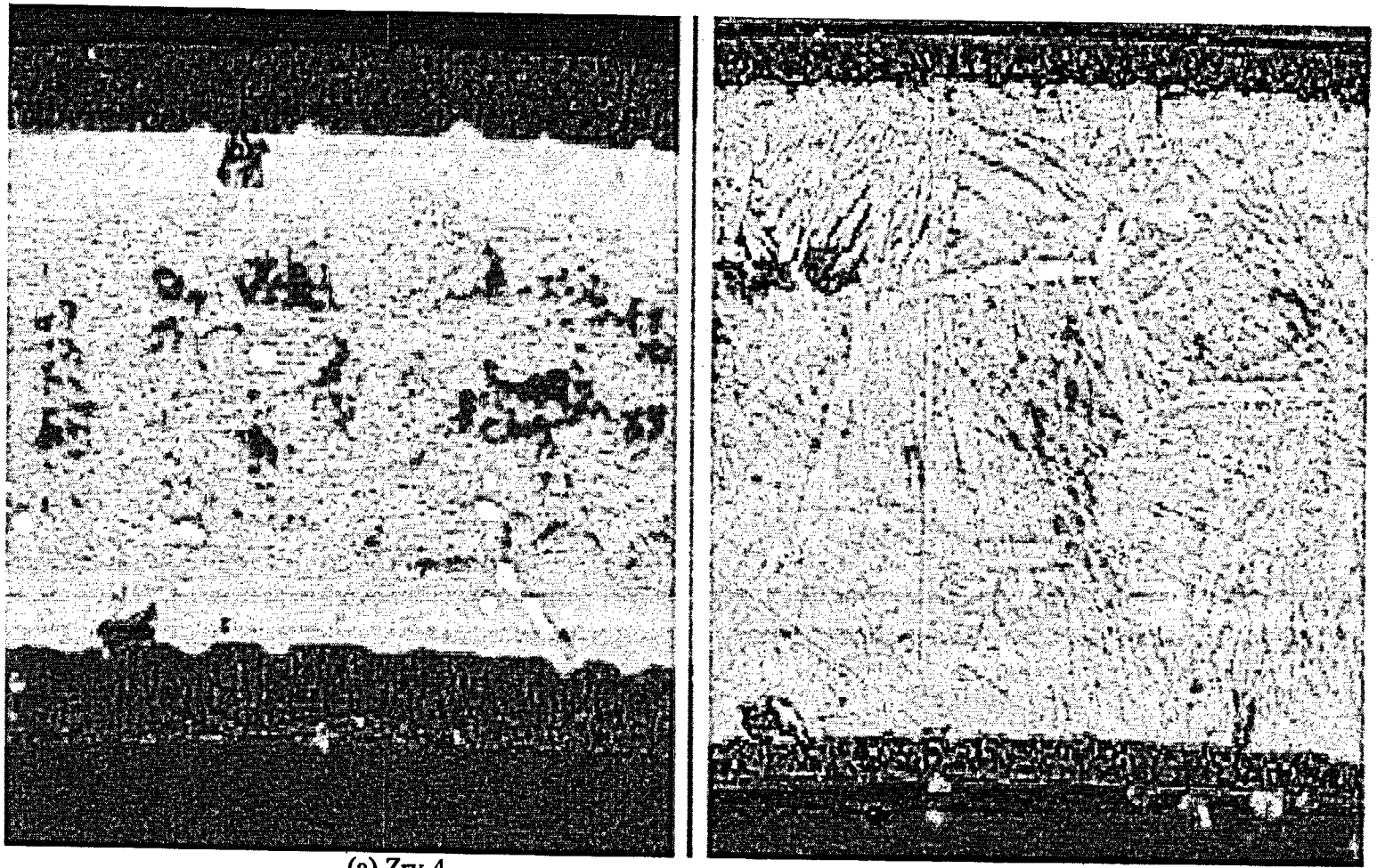

(a) Zry-4 (b) M5

Fig. 13. Metallography of as-polished Zry-4 (a) and M5 (b) oxidized in steam at 1000°C for ≈3400 s, slow cooled to 800°C and water quenched. Measured ECR values are 22.4% for Zry-4 and 13.3% for M5.

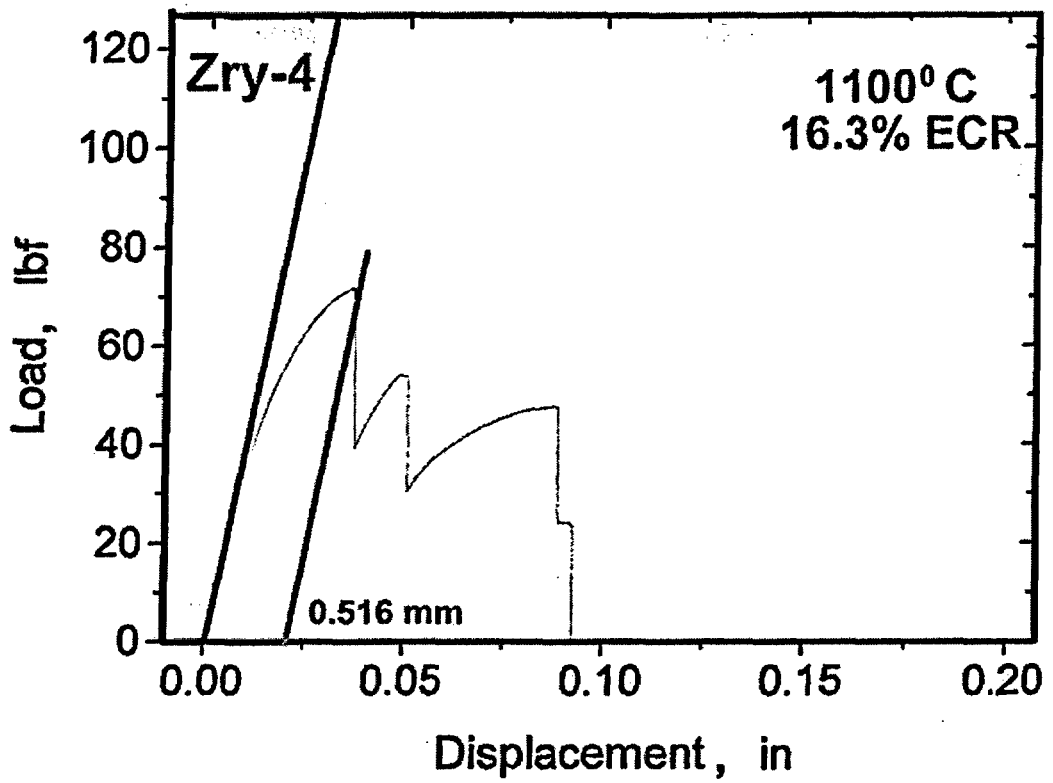

Fig. 14. Load-displacement curve for Zry-4 oxidized at 1100°C to a CP-calculated ECR of 15%, slow-cooled to 800°C and quenched to 100°C. The test was conducted on an 8-mm-long ring at room temperature and a cross-head displacement rate of 2 mm/minute. The offset displacement prior to the first through-wall crack is 0.516 mm.

Conclusions and Future Work

LOCA Integral Test Results for High-Burnup BWR Fuel

Metallography was conducted at several locations of the ICL#2 high-burnup LOCA integral sample to determine fuel morphology and Zry-2 cladding layer (oxide, alpha, and prior-beta) thicknesses. This sample had been pre-pressurized to ≈8.4 MPa at 300°C, ramped in flowing steam through ballooning and burst to 1204°C, held at 1204°C for 5 minutes, cooled to 800°C at 3°C/s and furnace-cooled from 800°C to room temperature. These destructive examinations were performed after significant handling of the LOCA specimen during nondestructive examinations and after the ballooned region had been filled with epoxy. Prior to this test, a companion out-of-cell test (OCL#11) had been conducted with nonirradiated Zry-2 (filled with zirconia pellets) to provide baseline data for the in-cell test. The condition of the fuel

below the balloon neck region appeared to be essentially the same as the pre-LOCA fuel structure of a sample sectioned from near the LOCA specimen. Some circumferential tearing of the post-LOCA fuel was observed at mid-radius, which may be due to the behavior of the high concentration of fission gas in this fuel ring and to the small expansion of the cladding away from the fuel. Fuel morphology was also imaged ≈50 mm above the burst center, ≈12 mm above the burst center and at the burst center. These results are interesting, but they are not necessarily indicative of the fuel morphology during the test. Essentially, these results demonstrate that the fuel cracks into small enough fragments that some axial relocation of fuel may occur during and/or following ballooning and burst. However, there is no evidence from the ICL#2 sample that the fuel mass per unit length increased within the ballooned region. In subsequent LOCA integral tests – with quench – the burst area will be taped prior to movement and handling to prevent fuel fallout. Also, gamma scanning will be performed to assess fuel relocation.

Based on measurements of cladding outer- and inner-surface oxide thickness at several axial locations, it appears that the presence of ≈10 μm of corrosion does not inhibit or slow down outer-surface oxidation and the presence of fuel and fuel-cladding bond does not retard inner surface steam oxidation. With regard to steam oxidation, high-burnup-fueled Zry-2 behaved very similar to nonirradiated Zry-2 during the LOCA transient. The major difference observed between post-LOCA high-burnup-fuel cladding and nonirradiated cladding was the degree of secondary hydriding in the balloon neck region: ≈4000 wppm hydrogen pickup for both necks of the nonirradiated cladding and ≈200 wppm for one neck of the high-burnup sample. A more detailed axial profile of hydrogen concentration and pickup will be obtained from the next high-burnup LOCA integral test (ICL#3) scheduled for December 2003. An additional test (ICL#4) with a high-burnup BWR fuel segment will be conducted – with quench – early in 2004 to generate a sample for post-quench-ductility testing. High-burnup PWR LOCA testing will be initiated following the ICL#4 test and maintenance at the LOCA hot-cell work station.

Advanced-Alloy Cladding Post-Quench Ductility

Zry-4, ZIRLO and M5 samples (25-mm-long) were oxidized at 1000°C and 1100°C to Cathcart-Pawel (CP) ECR values of 5-20%, slow cooled to 800°C and quenched. Rings (8-mm-long) cut from these samples were subjected to ring-compression testing at room temperature and a cross-head displacement rate of 2 mm/minute. All three alloys oxidized at 1100°C exhibited similar weight gains per time, which were consistent with CP-model predictions. At 1000°C, the ZIRLO and Zry-4 weight gains were within ±12% of the CP-predictions, with ZIRLO weight gain ≈10% lower and Zry-4 ≈12% higher than predicted for the longest test time (≈3400 s). These weight-gain differences scaled linearly with total oxide layer thickness for Zry-4 and ZIRLO. At 1000°C oxidation temperature, the M5 weight gain was ≈30% lower than predicted and ≈36% lower than the Zry-4 weight gain at ≈3400 s. The low weight gain of M5 under these conditions is due mostly to the slower growth rate of the inner- and outer-surface oxide layers. However, the M5/Zry-4 total-oxide ratio was less than the weight gain ratio, indicating more oxygen pickup in the M5 alpha and prior-beta regions. The resulting ECR values at 1000°C, based on measured weight gain, were 22% for Zry-4, 18% for ZIRLO and 13% for M5.

The results of the post-quench-ductility tests indicated that the three alloys oxidized at 1100°C had offset strains ≥4% at ≤17% CP-ECR. It was interesting to observe that all three alloys oxidized at 1000°C had ≈3% offset strain at 20% CP-ECR, even though the measured ECR values ranged from 13-22%. These results suggest that, for alloys oxidized at 1000°C, post-quench ductility correlates better with time-at-temperature, CP-calculated ECR and BJ-calculated ECR than with measured ECR. Microhardness and hydrogen analyses of these alloy samples are in progress, along with preparation of samples oxidized at 1200°C and 1260°C.

References

1. Y. Yan, R. V. Strain, T. S. Bray, and M. C. Billone, "High Temperature Oxidation of Irradiated Limerick BWR Cladding," Proceedings of the Nuclear Safety Research Conference (NSRC-2001), Washington, DC, October 22-24, 2001, NUREG/CP-0176 (2002) 353-372.

2. Y. Yan, R. V. Strain, and M. C. Billone, "LOCA Research Results for High-Burnup BWR Fuel," Proc. Nuclear Safety Research Conference (NSRC-2002), Washington, DC, October 28-30, 2002, NUREG/CP-0180 (2003) 127-155.

3. G. Hache and H. M. Chung, "The History of LOCA Embrittlement Criteria," Proc. 28th Water Reactor Safety Meeting, Bethesda, MD, October 23-25, 2000, NUREG/CP-0172 (2001) 205-237

4. W. J. Leech, "Ductility Testing of Zircaloy-4 and ZIRLO™ Cladding after High Temperature Oxidation in Steam," Proceedings of the Topical Meeting on LOCA Fuel Safety Criteria, Aix-en-Provence, 22-23 March, 2001, pp 135-143. http://www.nea.fr/html/nsd/docs/2001/csni-r2001-18.pdf

5. A. Le Bourhis, "Justification of the M5™ Behavior in LOCA," Proceedings of the Topical Meeting on LOCA Fuel Safety Criteria, Aix-en-Provence, 22-23 March, 2001, pp 105-133. http://www.nea.fr/html/nsd/docs/2001/csni-r2001-18.pdf

6. L. Yegorova, K. Lioutov, V. Smirnov, A. Goryachev, and V. Chesanov, "LOCA Behavior of E110 Alloy," these proceedings.